Applied Catalysis B: Environmental 179 (2015) 445–457

Contents lists available at ScienceDirect

Applied Catalysis B: Environmental

journal homepage: www.elsevier.com/locate/apcatb

Arylsulfonic acid functionalized hollow mesoporous carbon spheres for efficient conversion of levulinic acid or furfuryl alcohol to ethyl levulinate

Daiyu Song[b], Sai An[b], Bo Lu[b], Yihang Guo[a,*], Jiyan Leng[c,*]

[a] School of Environment, Northeast Normal University, Changchun 130117, PR China
[b] School of Chemistry, Northeast Normal University, Changchun 130024, PR China
[c] First Hospital of Jilin University, Jilin University, Changchun 130021, PR China

ARTICLE INFO

Article history:
Received 13 January 2015
Received in revised form 24 April 2015
Accepted 22 May 2015
Available online 6 June 2015

Keywords:
Ethyl levulinate
Biomass-derived platform molecule
Solid acid
Hollow mesoporous carbon sphere

ABSTRACT

A series of arylsulfonic acid functionalized hollow mesoporous carbon spheres ($ArSO_3H$-HMCSs) with controllable $ArSO_3H$ loadings (1.8 and 3.2 wt%) and inner diameters (120–260 nm) were successfully prepared by chemical bonding $ArSO_3H$ groups to furfuryl alcohol-derived hollow mesoporous carbon spheres *via* diazonium coupling. The morphology, textural properties and chemical structure of as-prepared $ArSO_3H$-HMCSs were well characterized by TEM, FESEM, nitrogen gas porosimetry measurement, XRD measurement, Raman scattering and FT-IR spectroscopy as well as XPS surface probe technique. As the novel solid acid catalysts, the catalytic activity and stability of the $ArSO_3H$-HMCSs were evaluated by synthesis of ethyl levulinate from biomass-derived platform molecules, levulinic acid or furfuryl alcohol. The obtained excellent acid catalytic activity in comparison of other carbon-based $-SO_3H$ catalysts such as $ArSO_3H$-functionalized ordered mesoporous carbon, sulfonated hollow mesoporous carbon spheres as well as sulfonated incompletely carbonized D-glucose and cellulose was explained in terms of their strong Brønsted acidity and perfect hollow nanospherical morphology with thin mesoporous shell.

1. Introduction

Efficient conversion of inexpensive and renewable biomass to industrially important chemicals is one of the most popular topics in green chemistry [1–8]. Homogeneous Brønsted acids such as H_2SO_4, HF and benzene sulfonic acid are essential catalysts for the above processes. Nevertheless, the use of these acids has drawbacks such as corrosion, difficulty in the separation of products and catalysts, acid-waste generation, environmental pollution and added extra cost [6,9]. It is one of the key technologies to establish environmentally-friendly approaches for the biomass conversion-related processes by designing efficient, separable, recyclable and low-cost solid acid catalysts [10,11].

Recently, sulfonic acid functionalized carbon-based solid acids have attracted particular attentions in environmentally benign biomass conversion processes. The materials can be easily prepared by incomplete carbonization of cheap sulfopolycyclic aromatic compounds in *conc.* H_2SO_4 or sulfonation of incompletely carbonized natural organic matter (*e.g.*, D-glucose, sucrose, cellulose and starch) [12–14]. Owing to strong Brønsted acidity and high density, these amorphous carbon materials bearing $-SO_3H$, —COOH and —OH groups function as the efficient solid acid catalysts for various acid-catalyzed reactions such as esterification, transesterification, hydration, and hydrolysis [12,13,15–18]. However, owing to the nonporous structure, bulk carbon-based $-SO_3H$ catalysts generally have very small BET surface area (less than 5 $m^2\ g^{-1}$) [13], which limits their catalytic activity due to disadvantages of lack of acid site numbers, poor accessibility of the acid sites as well as slow mass-transport rate. The problems are expected to be ameliorated by adjusting the morphological and textural properties of sulfonic acid functionalized carbon-based solid acids, which can influence the active site numbers, the accessibility of active sites on the catalyst surface and inside the pores to the substrates as well as mass-transport of the reactant or product molecules [19–24].

Motivated by the aforementioned ideas, in the present work, a series of novel carbon-based $ArSO_3H$ catalysts ($ArSO_3H$-HMCSs) with hollow mesoporous spherical morphologies and controllable $ArSO_3H$ loadings as well as inner diameters were successfully prepared by chemical bonding arylsulfonic acid groups to furfuryl alcohol-derived hollow mesoporous carbon spheres (HMCSs) *via*

* Corresponding authors. Tel.: +86 431 89165626; fax: +86 431 89165626.
E-mail address: guoyh@nenu.edu.cn (Y. Guo).

http://dx.doi.org/10.1016/j.apcatb.2015.05.047
0926-3373/

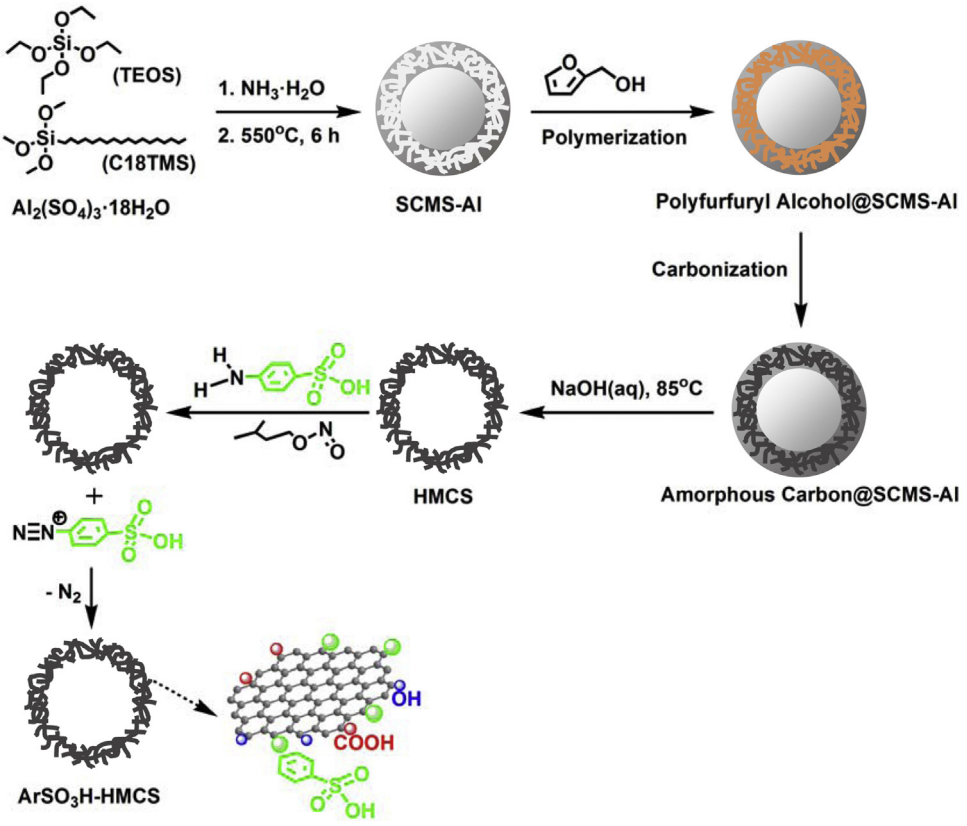

Scheme 1. Route of preparation of $ArSO_3H$-HMCSs materials.

diazonium coupling (Scheme 1). Hollow nanosphere catalysts with outstanding properties including hollow interiors, permeable and thin shells, shortened diffusion distance as well as unique textural properties (*e.g.*, very large BET surface area and porous structure) may significantly improve the accessibility of the active sites to the substrates, and thereby the enhanced catalytic activity of carbon-based —SO_3H catalysts in various chemical transformations is expected to be obtained.

To evaluate the heterogeneous acid catalytic performance of the $ArSO_3H$-HMCSs, synthesis of ethyl levulinate from esterification of levulinic acid and alcoholysis of furfuryl alcohol were selected as the model reactions. Ethyl levulinate is a member of alkyl levulinates family that is versatile chemical feedstocks with numerous applications in flavoring and fragrance industry or as a blending component in biodiesel [25,26]. The threat of an oil shortage is stimulating the search for alternative feedstocks to chemicals, and therefore, efficient conversion of biomass-derived levulinic acid or furfuryl alcohol to levulinate esters has attracted especial interests. For direct esterification of levulinic acid to produce levulinate esters, the byproduct water may inhibit the reaction to proceed effectively. An atom-economic and convenient method for the synthesis of alkyl levulinates can be envisioned by alcoholysis of furfuryl alcohol. For the aforementioned two reactions, development of efficient, separable and recyclable solid acid catalysts is the most important issue to establish environmentally sustainable approaches. Conventional solid acid catalysts including macroporous ion-exchange resins (*e.g.*, Amberlyst-15 or -70) [27,28], microporous zeolites (*e.g.*, HZSM-5) [29,30], mesoporous aluminosilicates (*e.g.*, Al-TUD-**1**) [31], sulfated metal oxides (*e.g.*, SO_4^{2-}/TiO_2 and SO_4^{2-}/ZrO_2) [28] and sulfonic acid-grafted silica (*e.g.*, SO_3H-SBA-15) [29,32] have been employed in synthesis of levulinate esters by esterification and ethanolysis reactions. However, the moderate yields of levulinate esters were obtained; additionally, catalyst deactivation was observed during recycling the solid acids.

To further evaluate the heterogeneous acid catalytic activity per acid site of the $ArSO_3H$-HMCSs, the reference acid catalysts including commercial Amberlyst-15, homogeneous benzene sulfonic acid and sulfuric acid as well as other SO_3H-functionalizd carbon-based materials like arylsulfonic acid functionalized ordered mesoporous carbon ($ArSO_3H$-OMC), sulfonated HMCSs (SO_3H-HMCSs) and cellulose- or D-glucose-derived carbon solid acid (SO_3H-CC or SO_3H-GC) prepared by partial carbonization of a microcrystalline cellulose powder or D-glucose and then sulfonation of the resulting carbon precursor in *conc.* H_2SO_4, respectively, were also tested. Additionally, influence of $ArSO_3H$ loadings and inner diameters of the hollow spherical $ArSO_3H$-HMCSs on the catalytic activity was studied. Based on the above results, influence of morphological and textural properties on the heterogeneous acid catalytic activity of carbon-based —SO_3H catalysts was revealed.

2. Experimental

2.1. Materials

Furfuryl alcohol (98%), sulfanilic acid (99%) and tetraethylorthosilicate (TEOS, 98%) were purchased from Sinopharm Chemical Reagent Co., Ltd. Octadecyltrimethoxysilane (C18TMS, 98%) was purchased from TCI. Isopentyl nitrite (96%) and levulinic acid (98%) were purchased from Sigma–Aldrich. Commercial Amberlyst-15 was purchased from Alfa Aesar. All other chemicals were analytical grade, and they were purchased from Beijing Fine Chemical Co. (China).

2.2. Catalyst preparation

2.2.1. Silica core/mesoporous aluminosilicate shell template (SCMS-Al)

The procedure was followed by the modified literature method [33]. Aqueous ammonia (25 wt%, 4 mL) was added to a solution containing ethanol (148 mL) and deinoized water (20 mL), and then TEOS (6, 10 or 20 mL, respectively, to obtain SCMS-Al templates with different solid core sizes) was added into the above solution at 30 °C under vigorous stirring. The mixture thus formed was kept stirring for 1 h to yield uniform silica spheres. Subsequently, the mixture containing TEOS (5 mL), C18TMS (2 mL) and $Al_2(SO_4)_3{\cdot}18H_2O$ (0.45 mol L^{-1}, 1 mL) was added to the above silica spheres-containing suspension and followed by further reacting for 1 h. The resulting C18TMS-incorporated SCMS-Al nanocomposite was retrieved by centrifugation, dried at 100 °C, and then calcined at 550 °C for 6 h under air atmosphere to produce the SCMS-Al template.

At molar composition of the starting materials in the preparation system of total TEOS:$Al_2(SO_4)_3{\cdot}18H_2O$:C18TMS = 0.049 :0.45:0.0047, the resulting template is denoted as SCMS-Al-**1**; similarly, at molar composition of 0.067:0.45:0.0047 and 0.112:0.45:0.0047, the resulting templates are denoted as SCMS-Al-**2** and SCMS-Al-**3**, respectively.

2.2.2. Hollow mesoporous carbon spheres (HMCSs)

SCMS-Al-**1** (0.5 g) was impregnated with furfuryl alcohol (0.7 mL), and the resulting mixture was air-dried at 60 °C for 3 h and then vacuum-dried at 60 °C for 10 h to generate polyfurfuryl alcohol catalyzed by the aluminosilicate framework of SCMS-Al-**1**. As-formed polyfurfuryl alcohol was converted into carbon inside the mesopores in the SCMS-Al-**1** shells by pyrolysis at 600 °C for 4 h under nitrogen gas flow. HMCSs-**1** was then recovered by removing SCMS-Al-**1** template with NaOH aqueous solution (2 mol L^{-1}) at 85 °C, followed by complete water washing and dried at 100 °C overnight. HMCSs-**2** and HMCSs-**3** were also prepared using the above method in the presence of SCMS-Al-**2** and SCMS-Al-**3** templates. ICP-AES determination confirmed that Al was not found in the resulting HMCSs.

2.2.3. Arylsulfonic acid functionalized hollow mesoporous carbon spheres ($ArSO_3H$-HMCSs)

At 70 °C, HMCSs-**1** (1.0 g) was dispersed into the mixture of sulfanilic acid (8.4 or 1 mmol) and water (60 mL) under vigorous stirring. After stirring for 2 h, the mixture was cooled to 30 °C. Subsequently, isoamyl nitrite (8.4 or 1 mmol) was added dropwise into the above mixture, and stirring was applied continuously for 16 h. The product was isolated by centrifugation, and then the solid was washed multiple times with water, followed by ethanol washing to remove by-products and residual starting compounds. The final product was air-dried overnight at 100 °C, and it is denoted as $ArSO_3H$-HMCS*s*n-**1**. Herein, *n* is sulfur content (wt%) in the $ArSO_3H$-HMCS*s*n materials, which was determined by ICP-OES. Similarly, $ArSO_3H$-HMCS*s*n-**2** and $ArSO_3H$-HMCS*s*n-**3** materials were also prepared *via* diazonium coupling HMCSs-**2** and HMCSs-**3** with arylsulfonic acid groups.

2.2.4. Arylsulfonic acid functionalized ordered mesoporous carbon ($ArSO_3H$-OMC)

Ordered mesoporous carbon (OMC) was synthesized using SBA-15 silica as hard template and furfuryl alcohol as carbon source, and the preparation procedure was followed by the modified literature method [34]. Typically, 1.5 mL of furfuryl alcohol and a small quantity of oxalic acid were dissolved in 10 mL of alcohol. Then 1 g of SBA-15 silica powder was dispersed into the above solution. After evaporation of ethanol and polymerizing furfuryl alcohol at 70 °C, the residual unpolymerized furfuryl alcohol was evaporated at 150 °C. The obtained polyfurfuryl alcohol/SiO_2 composite was thermal-treated in N_2 at 800 °C to carbonize the polyfurfuryl alcohol. The silica template in the composite was removed by repeatedly washing with hot NaOH solution (2 mol L^{-1}).

Under vigorous stirring and at 70 °C, OMC (1.0 g) was dispersed into sulfanilic acid (8.4 mmol)-containing water (60 mL). After 2 h, the mixture was cooled to 30 °C. Subsequently, isoamyl nitrite (8.4 mmol) was added dropwise into the above mixture under vigorous stirring for 16 h. The product was isolated by centrifugation, and then it was washed multiple times with water, followed by ethanol washing to remove by-products and residual starting compounds. The final product was air-dried overnight at 100 °C.

2.2.5. Sulfonated HMCSs (SO_3H-HMCSs)

HMCSs-**1** (2 g) was heated in 40 mL of *conc.* H_2SO_4 (>96%) at 150 °C under N_2 gas flow for 15 h. The mixture was diluted with 100 mL of distilled water, and the black powder was collected by filtration. Afterwards, the solid was washed repeatedly with hot distilled water (85 °C) until impurities such as sulfate ions were no longer detected in washing water. The resulting black solid was dried at 100 °C.

2.2.6. Sulfonated cellulose-derived carbon (SO_3H-CC)

The preparation procedure was followed by the modified literature method [13]. The microcrystalline cellulose powder (20 g) was heated for 5 h at 450 °C under N_2 gas flow to produce black solid, which was then ground to a powder. The black powder (2 g) was then boiled in 40 mL of *conc.* H_2SO_4 (>96%) at 150 °C under N_2 gas flow. After heating for 15 h and then cooling to room temperature, the suspension was filtered to yield a black precipitate, which was washed repeatedly with hot distilled water (85 °C, 100 mL) until impurities such as sulfate ions were no longer detected in the effluent. The resulting black solid was dried at 100 °C.

2.2.7. Sulfonated D-glucose-derived carbon materials (SO_3H-GC)

The preparation procedure was followed by the modified literature method [13]. D-glucose powder (20 g) was heated for 5 h at 450 °C under N_2 gas flow to produce a black solid, which was then ground to a powder. The black powder (2 g) was then boiled in 40 mL of *conc.* H_2SO_4 (>96%) at 150 °C under N_2 gas flow. After heating for 15 h and then cooling to room temperature, the suspension was filtered to yield a black precipitate. The precipitate was washed repeatedly with hot distilled water (85 °C, 100 mL) until impurities such as sulfate ions were no longer detected in the effluent. The resulting black solid was dried at 100 °C.

2.3. Catalyst characterization

TEM and FESEM observations were performed on a JEM-2100F high resolution transmission electron microscope and XL-30 ESEM FEG field emission scanning electron microscope, respectively. Raman scattering spectra were recorded on a Jobin-Yvon HR 800 instrument with an Ar^+ laser source at 488 nm in a macroscopic configuration. Nitrogen porosimetry measurement was performed on a Micromeritics ASAP 2020 M surface area and porosity analyzer. XRD patterns were obtained on a D/max-2200 VPC diffractometer using Cu Kα radiation. FT-IR spectra were recorded on a Nicolet Magna 560 IR spectrophotometer. XPS was performed on a VG-ADES 400 instrument with Mg Kα-ADES source at a residual gas pressure of below 10^{-8} Pa. All the binding energies were referenced to the C 1s peak at 284.8 eV of the surface adventitious carbon. The Brønsted acid-site density of as-prepared $ArSO_3H$-HMCSs ($A_{titration}$, μeq g^{-1}) was determined by titration with NaOH

Table 1
Textural parameters and Brønsted acid-site density of various solid acid catalysts[a]

Catalyst	S_{BET}($m^2\ g^{-1}$)	D_p(nm)	V_p($cm^3\ g^{-1}$)	$A_{titration}$(μeq g^{-1})	Inner diameter[b](nm)
HMCSs-**1**	632	3.9	0.45	–	120–140
$ArSO_3H$-HMCS*s1.8*-**1**	478	3.9	0.33	531	120–140
$ArSO_3H$-HMCS*s3.2*-**1**	418	3.9	0.28	855	120–140
$ArSO_3H$-HMCS*s3.2*-**2**	544	3.9	0.41	918	140–160
$ArSO_3H$-HMCS*s3.2*-**3**	545	3.9	0.43	857	240–260
$ArSO_3H$-OMC*3.8*	353	3.9	0.22	1044	–
SO_3H-HMCS*s3.3*-**1**	416	3.9	0.28	874	–
SO_3H-CC*3.9*	5	–	–	1152	–
SO_3H-GC*3.7*	< 1	–	–	1098	–
Amberlyst-15[c]	50	–	–	4800	–

[a] Surface area (S_{BET}) was calculated using the Brunauer–Emmett–Teller equation; pore diameters (D_p) was calculated using Barrett–Joyner–Halenda desorption branch of the isotherms; pore volume (V_p) was accumulated up to $P/P_0 = 0.99$.
[b] Inner diameter was calculated in TEM images.
[c] Data was from Ref. [44].

solution (0.0090 mol L^{-1}), and the detailed procedures were followed by the literature work [35].

2.4. Catalytic tests

Esterification of levulinic acid with ethanol was carried out in a three-necked round bottomed glass flask fitted with a water cooled condenser. For this reaction, 88 mg (2 wt%) of air-exposed catalyst was added, and the reaction was performed under ethanol refluxing in air (78 °C) with levulinic acid (9.85 mmol) to ethanol (68.95 mmol) molar ratio of 1:7 and constant volume (5 mL).

Ethanolysis of furfuryl alcohol was carried out in an autoclave with a Teflon lining under the conditions of 120 °C, furfuryl alcohol (1.15 mmol) to ethanol (69.00 mmol) molar ratio of 1:60 and 1.5 wt% of catalyst; meanwhile, stirring was applied throughout the reaction.

The concentrations of the produced ethyl levulinate were determined periodically on a Shimadzu 2014C gas chromatograph fitted with a HP-INNOWAX capillary column and flame ionization detector. Ethyl laurate was applied as an internal standard. The catalytic activity of various acid catalysts was evaluated quantitatively by the yields of ethyl levulinate (Y, %) and turnover frequency (TOF, h^{-1}). Herein, $Y\ (\%) = (M_D/M_T) \times 100$, where M_D and M_T are the number of moles of ethyl levulinate produced and expected, respectively; $\mathrm{TOF}\ (h^{-1}) = [M_D/(A_{titration} \times m)] \times t^{-1}$, where m (g) is the mass of the catalyst used in the reaction, and t (h) is the reaction time. The intermediates produced during the catalytic processes were identified by a HP6890GC-5973MSD mass spectrometry coupled with gas chromatography.

3. Results and discussion

$ArSO_3H$-HMCSs were prepared by the following two steps (Scheme 1). Firstly, incompletely carbonized furfuryl alcohol-derived HMCSs were fabricated by SCMS-Al hard template method, while SCMS-Al template was obtained by the formation of solid silica core and mesoporous aluminosilicate shell successively. The silica core size of SCMS-Al could be adjusted easily and reproducibly by tuning the starting amount of TEOS, leading to SCMS-Al-**1**–SCMS-Al-**3** with core diameters of 120–140, 140–160 and 240–260 nm, respectively (see TEM result displayed in Fig. 1a–c). Secondly, *in situ* diazonium coupling procedure was applied to functionalize HMCSs materials with $ArSO_3H$ groups under mild reaction conditions, and the resulting $ArSO_3H$-HMCSs had inner diameters of 120–140, 140–160 and 240–260 nm (see TEM result displayed in Fig. 1e–h and Table 1), respectively. This simple method of preparation of $ArSO_3H$-HMCSs is more secure than that of other approaches in which carbon-based $-SO_3H$ catalysts were obtained by using *conc.* H_2SO_4. Additionally, arylsulfonic acid groups can provide stronger proton release ability, leading to the prepared $ArSO_3H$-HMCSs higher acid catalytic activity than sulfonated carbon-based materials.

3.1. Characterization of the catalysts

The morphologies of as-prepared SCMS-Al, HCMSs and $ArSO_3H$-HMCSs were firstly revealed by TEM observations. Fig. 1a–c display the core-shell structure of three SCMS-Al templates, and the estimated thickness of aluminosilicate shell is 10–15 nm; as for diameters of solid silica core, they are 120–140 nm, 140–160 nm and 240–260 nm, respectively, for SCMS-Al-**1**–**3**. In the case of SCMS-Al-**1**-templated HMCSs-**1**, its hollow spherical structure can be clearly observed from Fig. 1d. Moreover, the inner diameter of HMCSs-**1** is consistent with the SCMS-Al-**1** template. After functionalization of HMCSs with $ArSO_3H$ group, the hollow spherical structure remains intact (Fig. 1f–h); additionally, the inner diameter of the resulting $ArSO_3H$-HMCSs is the same as the diameter of the corresponding solid silica core of SCMS-Al template, *i.e.*, 120–140 nm, 140–160 nm and 240–260 nm, respectively, for $ArSO_3H$-HMCS*s3.2*-**1**–$ArSO_3H$-HMCS*s3.2*-**3**. In the case of their shell thickness, it is the same as the thickness of aluminosilicate shell, *i.e.*, 10–15 nm. The shell thickness of SCMS-Al is determined by the concentration of $Al_2(SO_4)_3{\cdot}18H_2O$ in the starting preparation systems. In current preparation systems, the concentration of $Al_2(SO_4)_3{\cdot}18H_2O$ is the same, accordingly, $ArSO_3H$-HMCS*s3.2*-**1**–$ArSO_3H$-HMCS*s3.2*-**3** possess the same shell thickness. FESEM measurement can support the above TEM observations, and homogeneous hollow nanospheres with inner diameters of 120–140 nm, 140–160 nm and 240–260 nm and shell thickness of 10–15 nm are visibly seen in Fig. 1j–l. Therefore, construction of the $ArSO_3H$-HMCSs materials with controllable inner diameters is realized by adjusting the diameter of the solid silica core of SCMS-Al templates.

The textural properties of HMCSs-**1** and $ArSO_3H$-HMCSs materials were studied by nitrogen gas porosimetry measurement. From the result shown in Fig. 2A it is found all tested materials display type IV isotherm with H2 hysteresis loops, and the capillary condensation steps occur at the relative pressure $P/P_0 = 0.4–0.8$ (HMCSs-**1**, $ArSO_3H$-HMCS*s1.8*-**1**, $ArSO_3H$-HMCS*s3.2*-**1** and $ArSO_3H$-HMCS*s3.2*-**2**) or 0.4–1.0 ($ArSO_3H$-HMCS*s3.2*-**3**). The result indicates that the tested samples possess mesoporosity with uniform pore diameter but interconnecting pore channel. The mesostructure of the shell is formed due to the structure directing function of C18TMS. The sharp BJH pore size distribution curves also confirm the well-distributed mesopores of HMCSs and $ArSO_3H$-HMCSs materials; additionally, the pore diameter of the shell of HMCSs and $ArSO_3H$-HMCSs centers at 3.9 nm (Fig. 2B).

The textual parameters calculated based on the nitrogen gas sorption isotherms are summarized in Table 1. It indicates that four

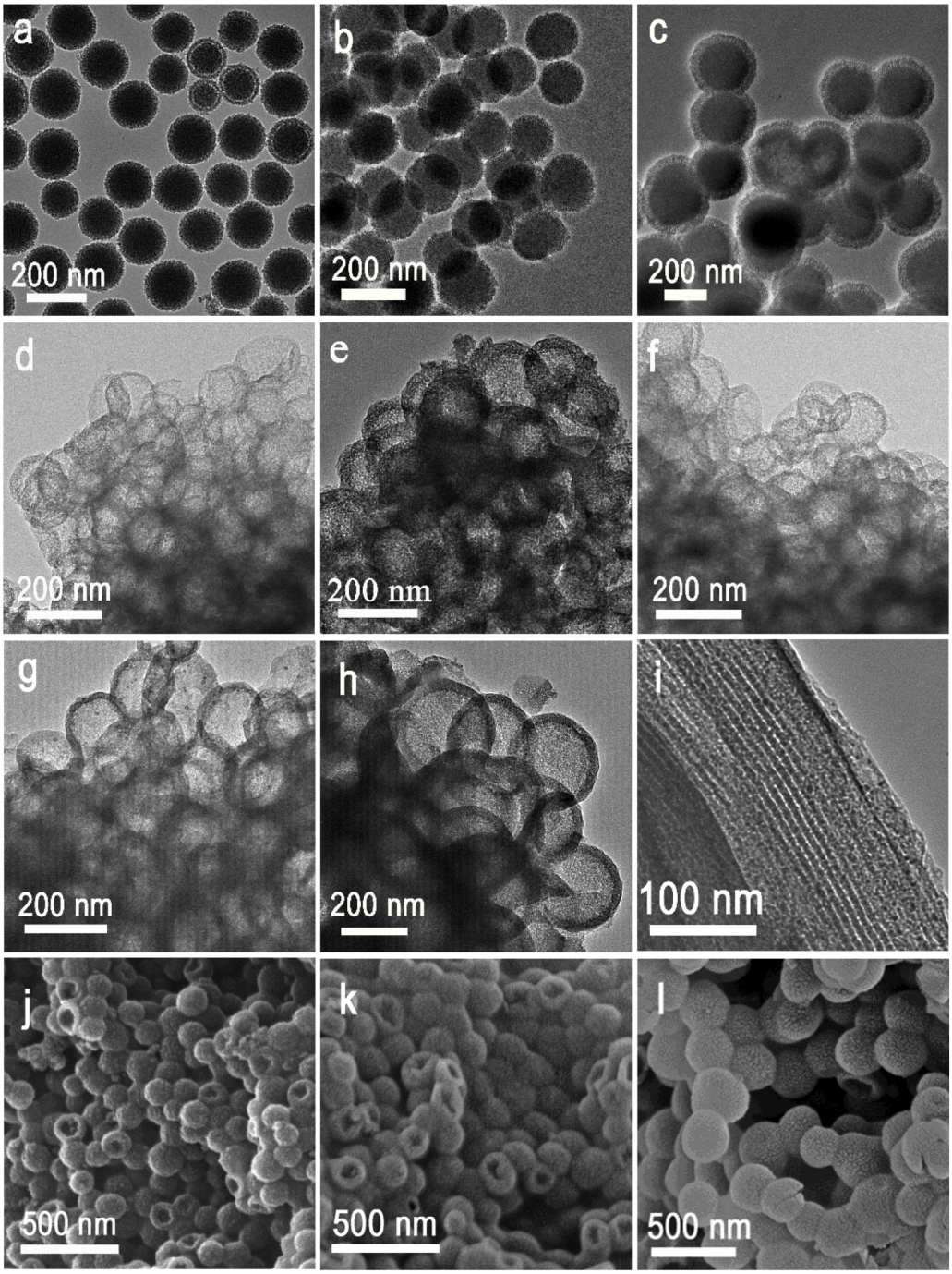

Fig. 1. TEM images of (a) SMCS-Al-**1**, (b) SMCS-Al-**2**, (c) SMCS-Al-**3**, (d) HMCSs-**1**, (e) $ArSO_3H$-HMCS*s1.8*-**1**, (f) $ArSO_3H$-HMCS*s3.2*-**1**, (g) $ArSO_3H$-HMCS*s3.2*-**2**, (h) $ArSO_3H$-HMCS*s3.2*-**3**, and (i) $ArSO_3H$-OMC*3.8*, and SEM image of (j) $ArSO_3H$-HMCS*s1.8*-**1**, (k) $ArSO_3H$-HMCS*s3.2*-**2**, and (l) $ArSO_3H$-HMCS*s3.2*-**3**.

as-prepared $ArSO_3H$-HMCSs possess very large BET specific surface area (418–545 $m^2\,g^{-1}$). However, compared with HMCSs, the BET specific surface area and pore volume decrease obviously after the incorporation of $ArSO_3H$ groups; moreover, the BET specific surface area and pore volume gradually decrease with increasing $ArSO_3H$ loading. For example, BET specific surface area of $ArSO_3H$-HMCS*s1.8*-**1** and $ArSO_3H$-HMCS*s3.2*-**1** are 478 and 418 $m^2\,g^{-1}$, and their pore volume are 0.33 and 0.28 $cm^3\,g^{-1}$, respectively. This is due to the fact that some of mesopores on the shell are blocked by $ArSO_3H$ groups. Interestingly, at the same $ArSO_3H$ loading (*i.e.*, 3.2 wt%), the BET specific surface area of $ArSO_3H$-HMCSs increases with their inner diameter from 120–140 nm to 140–160 nm; meanwhile, the pore volume also enhances. Further increasing the inner diameter to 240–260 nm, the BET specific surface area and pore volume of the resulting $ArSO_3H$-HMCS*s3.2*-**3** remain unchangeable. From Table 1 it is also found that at the similar $ArSO_3H$ loading, SO_3H-HMCS*s3.3*-**1** (416 $m^2\,g^{-1}$) has the same BET specific surface area as the $ArSO_3H$-HMCS*s3.2*-**1** (418 $m^2\,g^{-1}$). The excellent mesoporosity of as-prepared $ArSO_3H$-HMCSs materials originates from their hollow spherical nanostructure as well as mesoporous shell, which can provide both external and internal surface. In the cases of arylsulfonic acid functionalized $ArSO_3H$-OMC*3.8*, it possesses large BET specific surface area (353 $m^2\,g^{-1}$), however, its surface area is lower than its hollow spherical

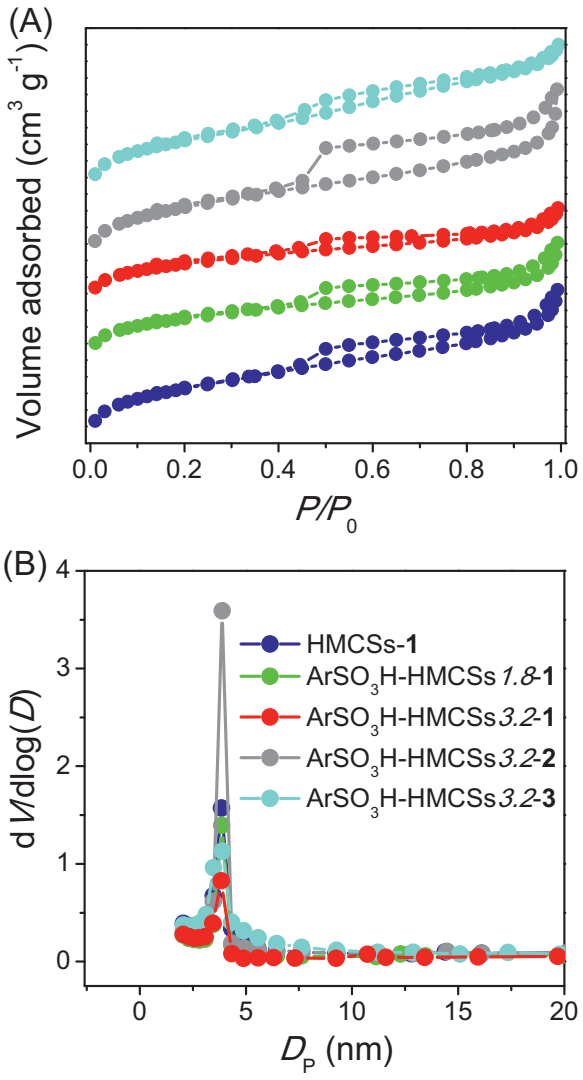

Fig. 2. Nitrogen gas adsorption/desorption isotherms (A) and pore size distribution curves (B) of HMCSs-**1** and various $ArSO_3H$-HMCSs materials.

counterpart. As for nonporous sulfonated cellulose- or D-glucose-derived bulk carbon materials, SO_3H-CC*3.9* (5 $m^2\ g^{-1}$) and SO_3H-GC*3.7* (lower than 1 $m^2\ g^{-1}$), their BET specific surface areas are very small.

XRD measurement (Fig. 3A), Raman scattering (Fig. 3B) and FT-IR (Fig. 3C) spectroscopies as well as XPS probe technique (Fig. 3D and E) were applied to study the chemical structure of the $ArSO_3H$-HMCSs. XRD patterns of HMCSs and $ArSO_3H$-HMCSs show two broad diffraction peaks at 10–32^0 (stronger) and 36–50^0 (weaker), which are assigned to the graphitic (0 0 2) and (1 0 1) planes, respectively. The result indicates that as-prepared HMCS-based materials are typical of amorphous carbon consisting of ordered and disordered polycyclic aromatic carbon sheets [13,18,36].

Raman scattering spectra agree well with the XRD result, and the scattering peaks found at 1334 (D band, corresponding to disordered sp^2 hybridized carbon network) and 1595 cm^{-1} (G band, corresponding to ordered sp^2 hybridized carbon network) are the characteristics of the carbonized materials with polycyclic aromatic carbon sheets [37,38]. From Raman scattering spectra it is also observed that the intensity ratio of D band to G band (I_D:I_G) significantly increases after functionalization of HMCSs with $ArSO_3H$ groups; moreover, the ratio (0.51, 0.65 and 0.76 for HMCSs, $ArSO_3H$-HMCSs*1.8*-**1** and $ArSO_3H$-HMCSs*3.2*-**1**) continuously increases with $ArSO_3H$ loading. As for the $ArSO_3H$-HMCSs*3.2*-**2** and $ArSO_3H$-HMCSs*3.2*-**3**, the ratio is 0.68 and 0.63, respectively, higher than that of HMCSs. The I_D:I_G ratio is applied to probe the degree of covalent functionalization of carbon materials [37,39], and enhanced I_D:I_G ratio of $ArSO_3H$-HMCSs with respect to HMCSs implies that $ArSO_3H$ groups are covalently bonded to the HMCSs framework *via* diazonium coupling reaction.

FT-IR analysis can further support the XRD and Raman scattering results. For the unfunctionalized HMCSs, the vibrational absorption peaks appeared at 3394, 2926 and 1710 cm^{-1} correspond to stretching vibrations of O—H, aliphatic C—H and C=O groups, respectively, indicating the presence of phenolic hydroxyl and carboxyl groups in the hollow spherical carbon material [34]. As for the peaks found at 1226, 1172 and 1585 cm^{-1}, they are assigned to C=C stretching vibrations, suggesting the presence of polycyclic aromatic carbon in HMCSs materials [34,37]. After functionalization of HMCSs with $ArSO_3H$ groups, the new absorption peaks show up at 1034 and 1005 cm^{-1}, which are ascribed to O=S=O and S=O stretching vibrations, respectively [18,39]; additionally, the peak intensities of C—H and C=O bond become weak obviously. The above results imply $ArSO_3H$ groups are successfully incorporated into the HMCSs framework.

XPS surface analysis is in line with the above FT-IR result, which can provide useful information concerning about $ArSO_3H$ groups and polycyclic aromatic carbon sheets in the $ArSO_3H$-HMCSs. By selecting $ArSO_3H$-HMCSs*3.2*-**1** as the representative sample, its high-resolution XPS spectra in the S2p and C1s binding energy regions are displayed in Fig. 3D and E. The S2p binding energy region can be deconvoluted into two pairs of peaks: the stronger pair of peaks are centered at the 168.2 eV [denoted as S2p$_{3/2}$(1)] and 169.2 eV [denoted as S2p$_{1/2}$(1)], respectively, corresponding to sulfonic acid groups of the $ArSO_3H$-HMCSs*3.2*-**1**; the weaker pair of peaks are centered at the 169.0 eV [denoted as S2p$_{3/2}$(2)] and 170.1 eV [denoted as S2p$_{1/2}$(2)], respectively, corresponding to the sulfonate (C—SO_3^-) in the $ArSO_3H$-HMCSs*3.2*-**1** [40,41].

The C1s binding energy region can be deconvoluted into four peaks: the main peak centered at 284.6 eV is assigned to sp^2-hybridized polycyclic aromatic carbon (C=C sp^2), while three small peaks centered at 286.8 eV, 287.9 eV and 288.1 eV originate from various surface functional groups of the $ArSO_3H$-HMCSs*3.2*-**1**, *i.e.*, C—OH, C=O and —COOH [40,42,43]. As a result, it is confirmed that $ArSO_3H$ groups are bonded to the HMCSs framework.

3.2. Catalytic performance of the catalysts

As-prepared $ArSO_3H$-HMCSs are successfully applied in conversion of biomass-derived platform molecules, levulinic acid or furfuryl alcohol, to ethyl levulinate (Scheme 2a and b). Firstly, $ArSO_3H$-HMCSs are applied in the synthesis of ethyl levulinate from esterification of levulinic acid with ethanol under the conditions of levulinic acid-to-ethanol molar ratio of 1:7, 2 wt% catalyst, 78 °C and atmospheric pressure. Fig. 4A displays the catalytic activity of various $ArSO_3H$-HMCSs materials in target reaction. It shows that for the $ArSO_3H$-HMCSs materials with the same inner diameter (*i.e.*, 120–140 nm) but different $ArSO_3H$ loadings, *i.e.*, $ArSO_3H$-HMCSs*1.8*-**1** and $ArSO_3H$-HMCSs*3.2*-**1**, their catalytic activity is determined by the acid site density. For example, the determined acid site density of $ArSO_3H$-HMCSs*1.8*-**1** and $ArSO_3H$-HMCSs*3.2*-**1** is 531 and 855 μeq g^{-1} (Table 1), and the yield of ethyl levulinate reaches 52.0 ($ArSO_3H$-HMCSs*1.8*-**1**) and 99.9% ($ArSO_3H$-HMCSs*3.2*-**1**), respectively, after the reaction proceeds for 4 h. The result suggests that $ArSO_3H$-HMCSs*3.2*-**1** with higher acid site density exhibits higher esterification activity than $ArSO_3H$-HMCSs*1.8*-**1** although the latter has larger BET surface area (Table 1). Additionally, for the $ArSO_3H$-HMCSs materials with the same $ArSO_3H$ loading (*i.e.*, 3.2 wt%) and similar acid site density but

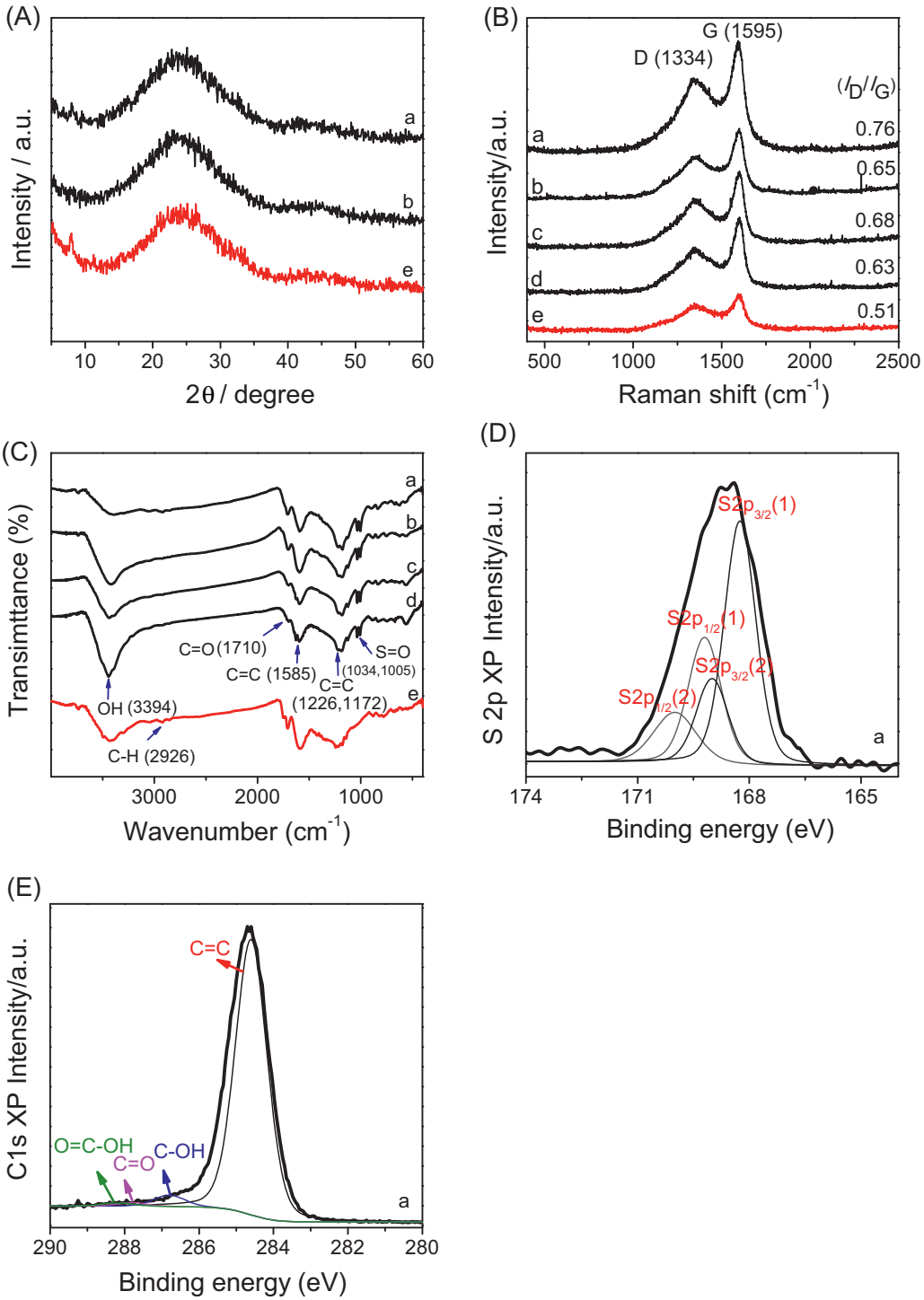

Fig. 3. XRD patterns (A), Raman scattering spectra (B), FT-IR spectra (C) and XPS (D and E) of various HMCS-based materials. (a) $ArSO_3H$-HMCS*s3.2*-**1**, (b) $ArSO_3H$-HMCS*s1.8*-**1**, (c) $ArSO_3H$-HMCS*s3.2*-**2**, (d) $ArSO_3H$-HMCS*s3.2*-**3** and (e) HMCS*s*-**1**.

different inner diameters of hollow spheres (*i.e.*, 120–140, 140–160 and 240–260 nm, respectively), *i.e.*, $ArSO_3H$-HMCS*s3.2*-**1**–$ArSO_3H$-HMCS*s3.2*-**3**, their catalytic activity is related to the inner diameters of hollow spheres. Larger inner diameter of hollow spheres leads to lower esterification activity although the former has larger BET surface area. For example, the yield of ethyl levulinate reaches 71.7 ($ArSO_3H$-HMCS*s3.2*-**3**), 82.0 ($ArSO_3H$-HMCS*s3.2*-**2**) and 99.9% ($ArSO_3H$-HMCS*s3.2*-**1**), respectively, after the reaction proceeds for 4 h. Therefore, $ArSO_3H$-HMCS*s3.2*-**1** with suitable inner diameter of hollow spheres and higher $ArSO_3H$ loading exhibits the highest esterification activity among the four tested $ArSO_3H$-HMCSs catalysts.

The esterification activity of $ArSO_3H$-HMCS*s3.2*-**1** is further compared with commercially available homogeneous (*i.e.*, benzene sulfonic acid and H_2SO_4) and heterogeneous (*i.e.*, macroreticular Amberlyst-15) Brønsted acid catalysts, and the result is shown in Fig. 4B. Owing to much higher Brønsted acid strength and acid site density, both benzene sulfonic acid and H_2SO_4 exhibit higher

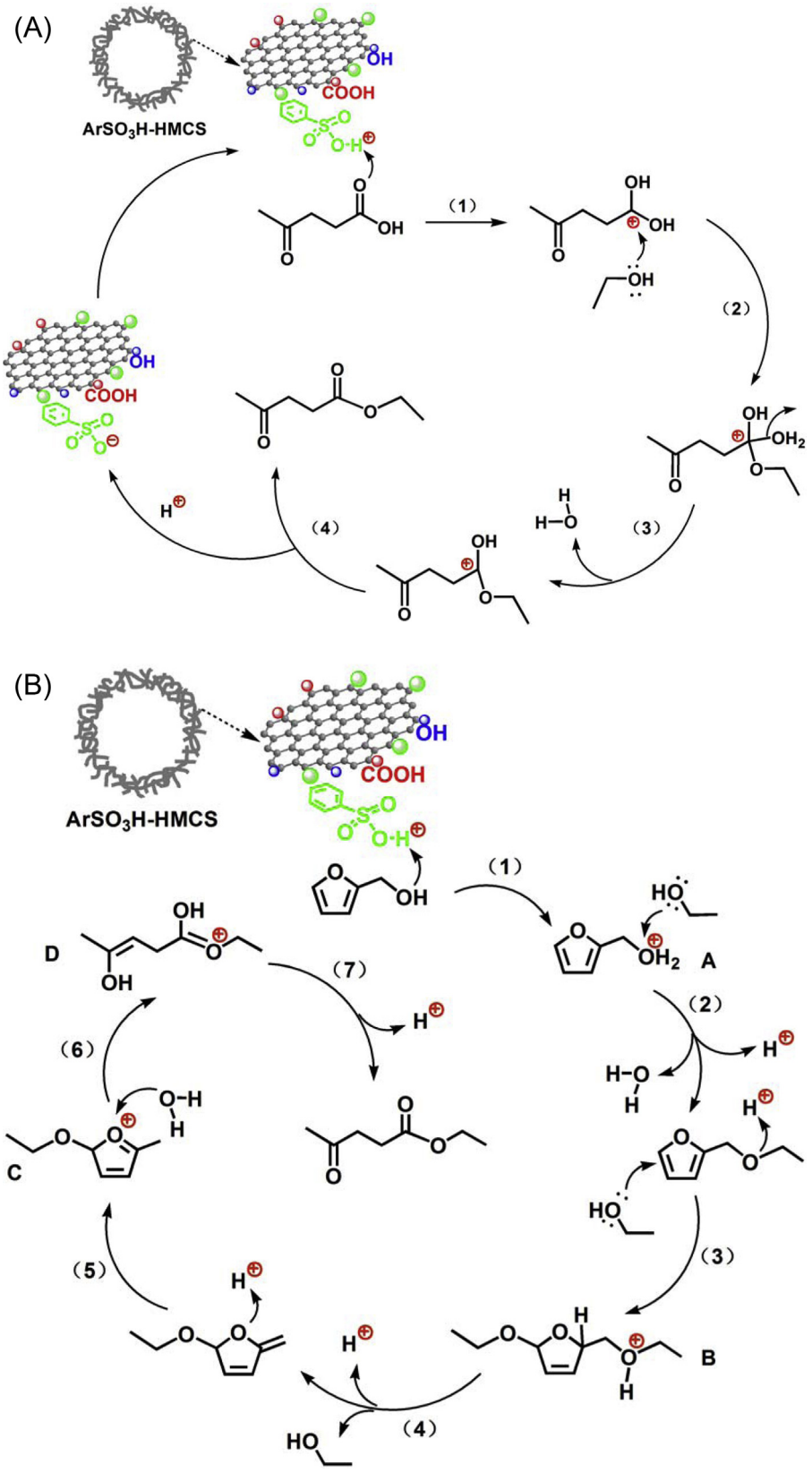

Scheme 2. (a) Possible mechanism of synthesis of ethyl levulinate from esterification of levulinic acid catalyzed over the $ArSO_3H$-HMCSs catalysts. (b) Possible mechanism of synthesis of ethyl levulinate from ethanolysis of furfuryl alcohol catalyzed over the $ArSO_3H$-HMCSs catalysts.

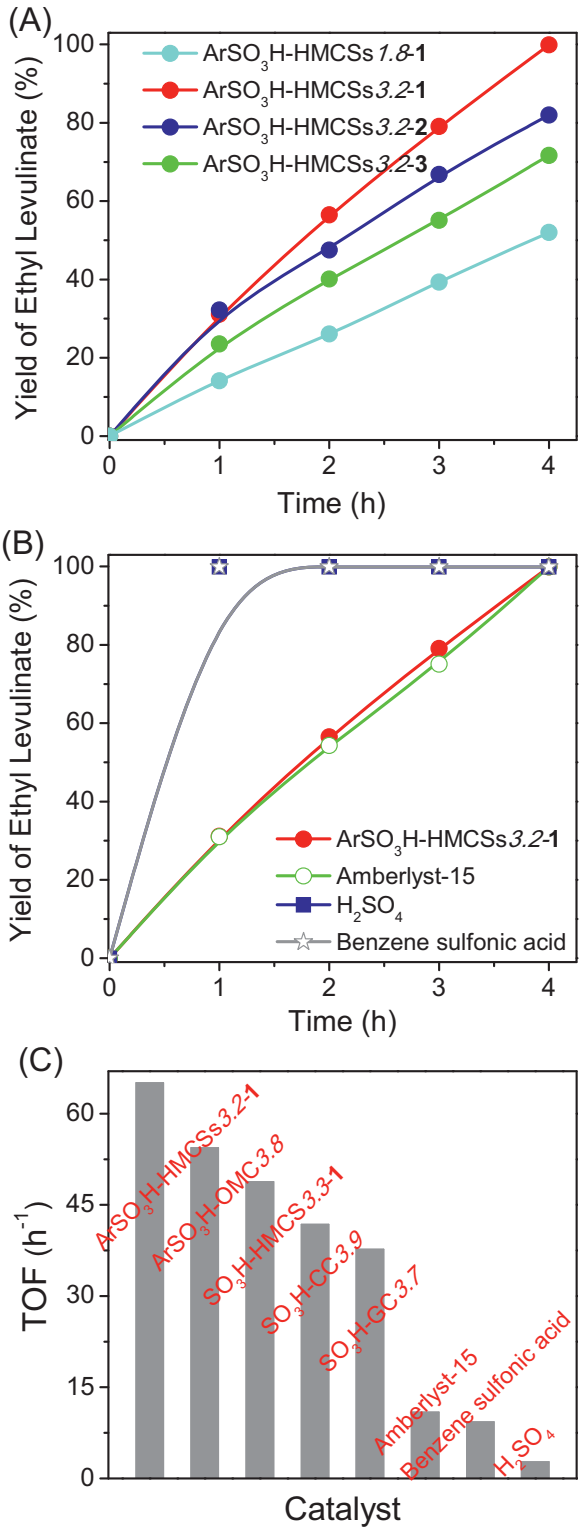

Fig. 4. Catalytic activity studies of various acid catalysts towards esterification of levulinic acid to ethyl levulinate. (A) $ArSO_3H$-HMCSs; (B) commercial acids; (C) carbon-based solid acids and commercial acids in terms of TOF (reaction time 2 h). Levulinic acid 9.85 mmol; ethanol 68.95 mmol; 2 wt% catalyst; 78 °C; atmospheric pressure.

catalytic activity than $ArSO_3H$-HMCS*s3.2*-**1**, and the yield of ethyl levulinate reaches *ca.* 100% after the reaction performs for 1 h. However, homogeneous benzene sulfonic acid and H_2SO_4 suffer from disadvantages such as corrosion, difficulty in the separation and acid-waste generation, leading to them uncompetitive with respect to solid acids. As for Amberlyst-15, its esterification activity is comparable to $ArSO_3H$-HMCS*s3.2*-**1**.

Considering the influence of Brønsted acid density on the acid catalytic activity, the esterification activity of $ArSO_3H$-HMCS*s3.2*-**1** is also compared with other SO_3H functionalized carbon-based catalysts (*i.e.*, SO_3H-HMCS*s3.3*, $ArSO_3H$-OMC*3.8*, SO_3H-CC*3.9* and SO_3H-GC*3.7*) and the aforementioned commercially available acid catalysts in terms of the yield of ethyl levulinate per acid site (*i.e.*, TOF, h^{-1}). From the result shown in Fig. 4C it is found that the TOF value of the tested acid catalysts follows the order $ArSO_3H$-HMCS*s3.2*-**1** > $ArSO_3H$-OMC*3.8* > SO_3H-HMCS*s3.3*-**1** > SO_3H-CC*3.9* > SO_3H-GC*3.7* > Amberlyst-15 > benzene sulfonic acid > H_2SO_4. Lower TOF value but higher yield of benzene sulfonic acid, H_2SO_4 and Amberlyst-15 is due to their high Brønsted acid site density.

Subsequently, the heterogeneous acid catalytic activity of as-prepared $ArSO_3H$-HMCSs materials is tested in ethanolysis of furfuryl alcohol to synthesize ethyl levulinate. At first, influence of reaction temperature on the ethanolysis activity is studied by selecting $ArSO_3H$-HMCS*s3.2*-**1** as the representative catalyst, and the result is displayed in Fig. 5A. After the reaction carries out for 120 min, the yield of ethyl levulinate increases from 52.3, 81.3 to 85.9% as increasing the reaction temperature from 100, 120 to 140 °C. In the following catalytic tests, the temperature of the ethanolysis reaction is set at 120 °C to ensure considerably high catalytic activity at relatively low reaction temperature.

Afterwards, influence of furfuryl alcohol-to-ethanol molar ratio on the ethanolysis activity was tested by selecting $ArSO_3H$-HMCS*s3.2*-**1** as the representative catalyst. From the result shown in Fig. 5B it can be seen that changing the molar ratio from 1:30, 1:45 to 1:60, the yield of ethyl levulinate continuously increases from 60.0, 63.8 to 81.3% after the reaction carried out for 120 min at 120 °C. However, further increasing the molar ratio to 1:75, the yield decreases to 68.7%. This is due to the fact that lower concentration of ethanol in the catalytic system could induce partial polymerization of furfuryl alcohol molecules [29]; meanwhile, excessive ethanol may dilute the substrate. Both of the factors results in the decreased ethyl levulinate yield.

Next, under the conditions of 120 °C and furfuryl alcohol-to-ethanol molar ratio of 1:60, the ethanolysis activity of various $ArSO_3H$-HMCSs materials with different $ArSO_3H$ loadings and inner diameters of hollow spheres is tested. From the result presented in Fig. 6A it is found that four as-prepared $ArSO_3H$-HMCSs materials (*i.e.*, $ArSO_3H$-HMCS*s1.8*-**1**, $ArSO_3H$-HMCS*s3.2*-**1**–$ArSO_3H$-HMCS*s3.2*-**3**) showed considerably high ethanolysis activity. Over period of 120 min, the yield of ethyl levulinate reached 64.6 ($ArSO_3H$-HMCS*s1.8*-**1**), 81.3 ($ArSO_3H$-HMCS*s3.2*-**1**), 71.5 ($ArSO_3H$-HMCS*s3.2*-**2**) and 69.3% ($ArSO_3H$-HMCS*s3.2*-**3**), respectively. In line with the $ArSO_3H$-HMCSs-catalyzed esterification reaction, the ethanolysis activity of the $ArSO_3H$-HMCSs is also related to the $ArSO_3H$ loading and inner diameter of hollow spheres: higher $ArSO_3H$ loading or smaller inner diameter leads to the catalyst with higher ethanolysis activity. However, further extending the reaction time didn't obtain the obviously increased yield of ethyl levulinate. The result implies that by-products or intermediates may produce in the reaction system, accompanying with the formation of ethyl levulinate. Therefore, GC-MS analysis is carried out to identify the by-products or intermediates yielded in current reaction system. As expected, the intermediate, ethoxymethylfuran, together with some oligomeric condensation products of furfuryl alcohol are identified (Fig. S1 of electronic

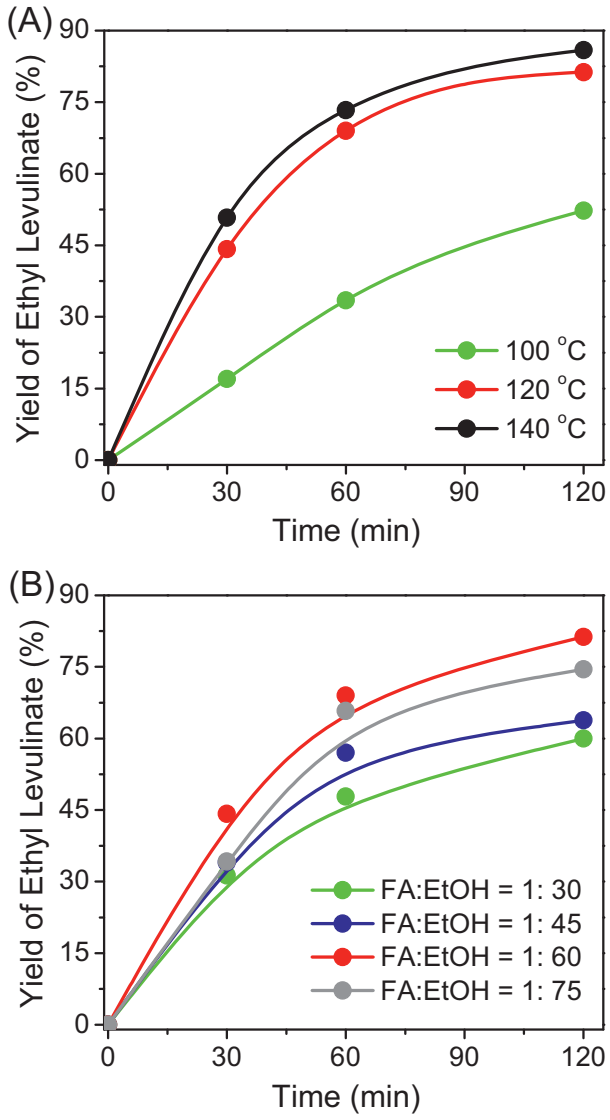

Fig. 5. Influence of reaction temperature (A) and furfural alcohol-to-ethanol molar ratio (B) on the catalytic activity of $ArSO_3H$-HMCS*s3.2*-**1** in ethanolysis of furfuryl alcohol to ethyl levulinate. Furfuryl alcohol 1.15 mmol; ethanol 69.00 mmol; 1.5 wt% catalyst. For Fig. B, the reaction was performed at 120 °C.

supplementary information). Formation of these compounds may decrease the selectivity of $ArSO_3H$-HMCSs, thereby limiting further increase of the activity.

The ethanolysis activity of $ArSO_3H$-HMCS*s3.2*-**1** is also compared with benzene sulfonic acid, H_2SO_4 and Amberlyst-15, and the result is shown in Fig. 6B. During the initial stage of the ethanolysis reaction, the yield of ethyl levulinate increases rapidly in homogeneous benzene sulfonic acid- or H_2SO_4-catalyzed reaction system. For example, the yield of ethyl levulinate reached 76.0% and 65.0%, respectively, over period of 60 min. However, further increasing the reaction time to 120 min, the ethanolysis activity remains unchangeable, which originates from the formation of many oligomeric condensation products of furfuryl alcohol in both of the systems [1]. Heterogeneous Amberlyst-15 exhibited excellent catalytic performance to the target reaction, and the yield of ethyl levulinate reaches 92.4% after the reaction proceeds for 60 min; meanwhile, only small amount of oligomeric condensation products of furfuryl alcohol are found. The higher catalytic activity of Amberlyst-15 than $ArSO_3H$-HMCSs is due to its much higher

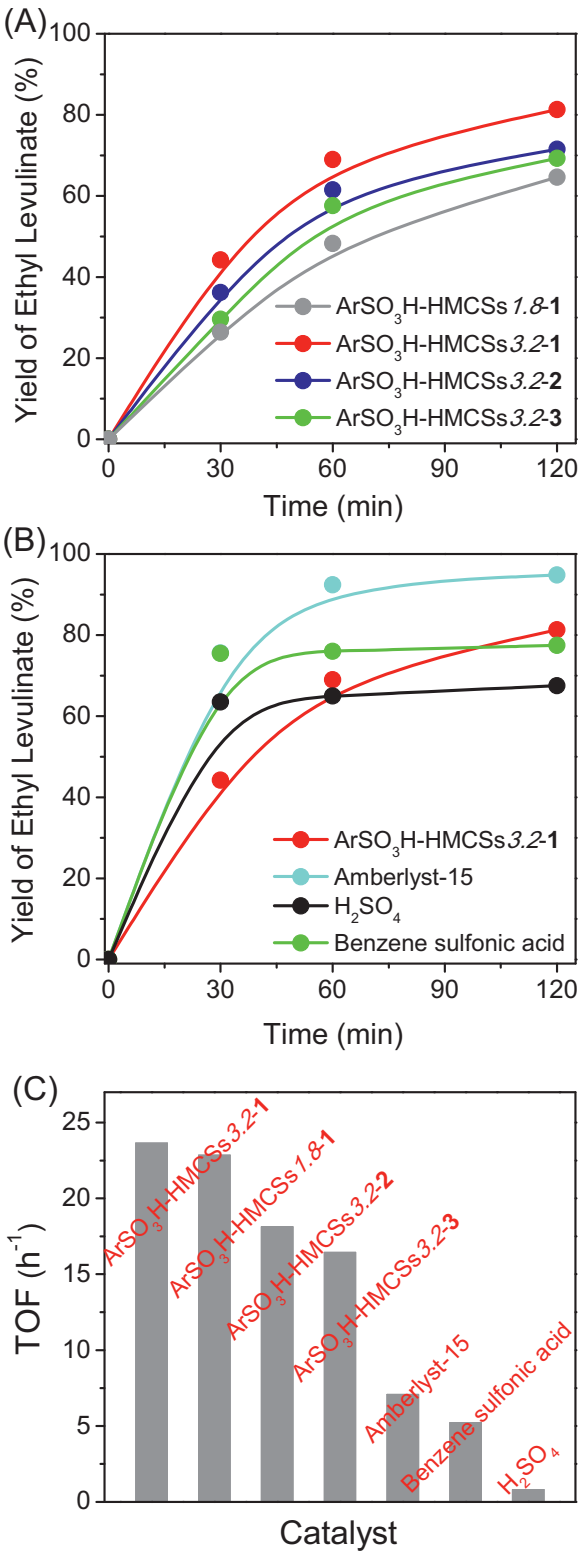

Fig. 6. Catalytic activity studies of various acid catalysts towards ethanolysis of furfural alcohol to ethyl levulinate. (A) $ArSO_3H$-HMCSs; (B) commercial acids; (C) carbon-based solid acids and commercial acids in terms of TOF. Furfuryl alcohol 1.15 mmol; ethanol 69.00 mmol; 1.5 wt% catalyst; 120 °C.

Brønsted acid site density (4800 μeq g^{-1}), which can provide much more acid sites for the target reaction.

Since the above tested acid catalysts possess different acid site densities (Table 1), the ethanolysis activity of various carbon-based solid acids and commercial acids are further compared in terms of the yield of ethyl levulinate per acid site (*i.e.*, TOF, h^{-1}), and the result is provided in Fig. 6C. It shows that the catalysts follow ethanolysis activity (TOF) order $ArSO_3H$-HMCSs*3.2*-**1** > $ArSO_3H$-HMCSs*1.8*-**1** > $ArSO_3H$-HMCSs*3.2*-**2** > $ArSO_3H$-HMCSs*3.2*-**3** > Amberlyst-15 > benzene sulfonic acid > H_2SO_4, and the corresponding TOF values are 23.6, 22.9, 18.1, 16.4, 7.1, 5.2 and 0.8 h^{-1}, respectively. The high yield but low TOF value of Amberlyst-15 is due to its extremely high acid site density (4800 μeq g^{-1}) [44]. Therefore, as-prepared $ArSO_3H$-HMCSs, regardless of $ArSO_3H$ loading, are more active than Amberlyst-15 in terms of the activity per acid site.

3.3. Discussion

The excellent acid catalytic activity of $ArSO_3H$-HMCSs is explained by the combination of strong Brønsted acid properties and unique hollow nanospherical morphology as well as well-defined mesoporosity.

Carbon-based $-SO_3H$ catalysts are composed of numerous graphene sheets with phenolic OH and COOH groups in addition to $-SO_3H$ groups. Some $-SO_3H$ groups interact with adjacent phenolic OH or COOH groups *via* strong hydrogen bonding [45]. The strong hydrogen bonding between the hydrophilic reactants (levulinic acid, furfuryl alcohol or ethanol) and the OH or COOH groups of the carbon materials promotes reactivity in contrast to Amberlyst-15 with hydrophobic backbones that would repel the reactants. The mutual electron-withdrawal owing to hydrogen bonding can result in them strong proton release ability and thereby high Brønsted acid strength. The excellent Brønsted acid properties allow esterification of levulinic acid and ethanolysis of furfuryl alcohol to proceed at considerably fast rate; meanwhile, strong Brønsted acid sites tend to favor the formation of ethyl levulinate for the aforementioned target reactions. For the $ArSO_3H$-HMCSs-catalyzed esterification reaction, protonation of carbonyl groups of levulinic acid molecules by $-SO_3H$ groups is the first step, which give oxonium ions that are readily attacked by ethanol molecules through an exchange reaction to produce ethyl levulinate molecules after losing one hydrogen atom (Scheme 2a) [46].

In the case of the $ArSO_3H$-HMCSs-catalyzed ethanolysis reaction, protonation of hydroxyl groups of furfuryl alcohol molecules by $-SO_3H$ groups to yield oxonium ions (intermediate A) is the first step. Subsequently, the oxonium ions are attracted by ethanol to form ethoxymethylfuran (detected by GC-MS) and water (step 2). In the third step, intermediate B is formed in the presence of $-SO_3H$ groups and ethanol. After being withdrawn one ethanol molecule and one hydrogen atom, 2-ethoxy-5-methylene-2,5-dihydrofuran (detected by GC–MS) is formed (step 4). In the presence of strong Brønsted acid sites, the protonation of epoxy groups of 2-ethoxy-5-methylene-2,5-dihydrofuran took place, giving rise to cyclic oxonium (step 5). Afterwards, the ring-open reaction occurs *via* water molecules attacking intermediate C, which produces intermediate D. Finally, the intermediate D is isomerized, together with releasing one hydrogen atom, which leads to ethyl levulinate (step 7) [1]. After this catalytic cycle, the catalyst restores its initial state by obtaining one hydrogen atom. The above procedure is illustrated in Scheme 2b.

Additionally, in comparison of sulphonated SO_3H-HMCSs*3.3*-**1** with $ArSO_3H$-functionalized $ArSO_3H$-HMCSs*3.2*-**1**, aryl groups in the latter also can provide electron-withdrawal environments, leading to $ArSO_3H$-HMCSs*3.2*-**1** higher esterification activity than SO_3H-HMCSs*3.3*-**1** although they both possess the hollow spherical nanostructure and very similar acid site density (874 and 855 μeq g^{-1}, Table 1) as well as textural properties.

On the other hand, to a great extent, the heterogeneous acid catalytic activity of the carbon-based $-SO_3H$ catalysts is dominated by their morphological and textural properties. For example, the Brønsted acid site density of mesoporous bulk $ArSO_3H$-OMC*3.8* (1044 μeq g^{-1}) is higher than its hollow spherical analog $ArSO_3H$-HMCSs*3.2*-**1** (855 μeq g^{-1}), however, its esterification activity is relatively low. For $ArSO_3H$-HMCSs catalysts, their unique hollow nanospherical morphology with thin shell can serve as the nanoreactors to permit esterification or ethanolysis reaction taking place inside. Accordingly, the diffusion path of the reactants and products is shortened, leading to the increased accessibility of $ArSO_3H$ sites to levulinic acid or furfuryl alcohol molecules. Finally, mass transport of the reactants and products can be speeded up, which results in the enhancement of the esterification or ethanolysis activity.

Additionally, hollow spherical nanostructure of $ArSO_3H$-HMCSs leads to them excellent mesoporosity with large BET surface area (418, 544 and 545 m^2 g^{-1} for $ArSO_3H$-HMCSs*3.2*-**1**–$ArSO_3H$-HMCSs*3.2*-**3**), well-distributed pores and high pore volume, which can provide better dispersion of the $ArSO_3H$ sites throughout the shell of the catalysts and increase the population of the acid sites. As a consequence, the accessibility of the reactant molecules to the $ArSO_3H$ sites also can be increased, giving a positive influence on their acid catalytic activity. However, for the mesostructured bulk $ArSO_3H$-OMC*3.8*, although it has well-defined mesostructure, its BET surface area (353 m^2 g^{-1}) is smaller than its hollow spherical analog. Additionally, the lengthened diffusion and transport pathway (pore channels of bulk mesoporous material are longer) limits its catalytic activity, leading to it lower acid-catalytic activity compared with its hollow nanospherical analog.

As for two sulfonated bulk carbon based catalysts, SO_3H-CC*3.9* and SO_3H-GC*3.7*, they have similar acid site density with the SO_3H-HMCSs*3.3*-**1**, and their poor catalytic activity is due to nonporous bulk structure, leading to them inferior textural properties with very small BET surface area (lower than 5 m^2 g^{-1}). Accordingly, the accessibility of SO_3H sites to the reactant molecules is limited significantly.

In the cases of three spherical $ArSO_3H$-HMCSs*3.2* catalysts, $ArSO_3H$-HMCSs*3.2*-**1**–$ArSO_3H$-HMCSs*3.2*-**3**, their activity difference in both esterification and ethanolysis reactions is due to their different inner diameters. The diffusion path of the reactants and products of $ArSO_3H$-HMCSs*3.2*-**3** with the largest inner diameter is the longest, and thereby the lowest activity among the three $ArSO_3H$-HMCSs*3.2* catalysts is found.

For the reference catalyst, Amberlyst-15, it has extremely high Brønsted acid site density, resulting in it much higher yield of ethyl levulinate in both esterification and ethanolysis reactions. However, considering catalytic activity per acid site, it has the lowest TOF value among all tested carbon-based $-SO_3H$ catalysts.

3.4. Reusability of the catalysts

The catalytic stability of as-prepared $ArSO_3H$-HMCSs is studied by esterification of levulinic acid with ethanol catalyzed by the representative catalyst, $ArSO_3H$-HMCSs*3.2*-**1**, and the reaction is repeated for ten times. For comparison, the reusability of Amberlyst-15 is also tested under the same conditions. After each catalytic cycle, the used catalyst is recovered by centrifugation, washed thoroughly with ethanol for three times, and dried at 100 °C prior to the next cycle. As shown in Fig. 7A, the activity loss of $ArSO_3H$-HMCSs*3.2*-**1** catalyst is neglectable after ten cycles, and the yield of ethyl levulinate maintains at *ca.* 80% after the reaction carries out for 3 h. Similarly, Amberlyst-15 also shows excellent

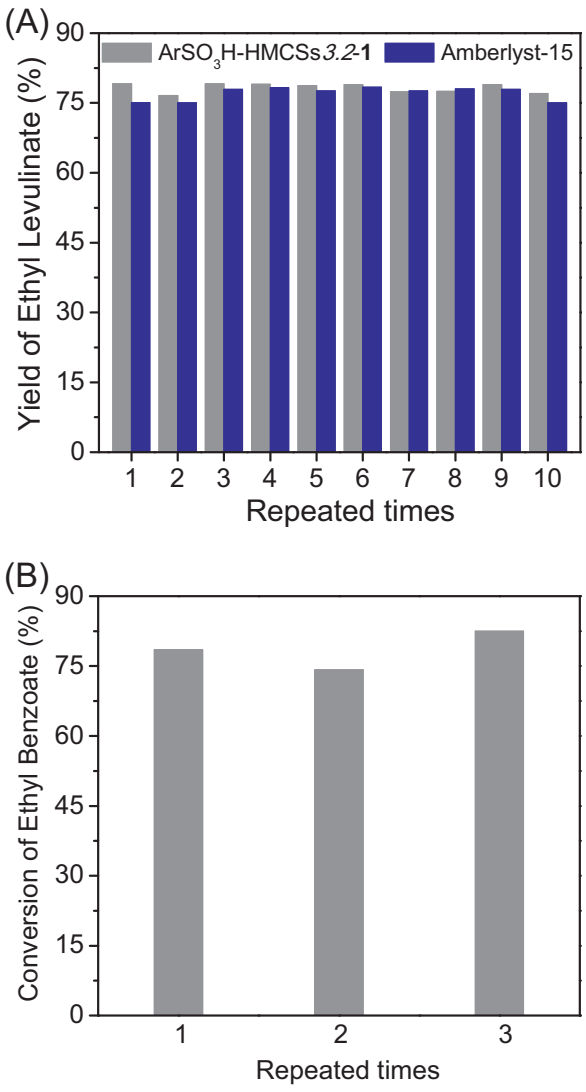

Fig. 7. Reusability of $ArSO_3H$-HMCS*s3.2*-**1** towards esterification (A) and hydrolysis (B) reactions. Condition for esterification reaction: levulinic acid 9.85 mmol; ethanol 68.95 mmol; 2 wt% catalyst; 78 °C; atmospheric pressure; 3 h. Condition for hydrolysis reaction: ethyl benzoate 1.29 mmol; water 450 mmol; acetonitrile 40 mmol; 0.67 wt% catalyst; 80 °C; atmospheric pressure; 2 h.

catalytic stability to the traget reaction, and it can maintain the original activity after ten consecutive cycles.

Additionally, in order to evaluate the catalytic stability of as-prepared $ArSO_3H$-HMCSs in the presence of water in reaction media, the representative $ArSO_3H$-HMCS*s3.2*-**1** catalyst is further tested in hydrolysis of ethyl benzoate at 80 °C. From the result shown in Fig. 7B it is found that the $ArSO_3H$-HMCS*s3.2*-**1** still maintains excellent catalytic stability in the presence of water, and conversion of ethyl benzoate is 78.5, 74.2 and 82.5%, respectively, for the first, second and third run. Meanwhile, elution of SO_3H groups into the reaction media is hardly detected by ICP–OES. Both of the results confirm the excellent catalytic stability of the $ArSO_3H$-HMCSs in ester hydrolysis reaction except in esterification reaction. The excellent catalytic stability of the $ArSO_3H$-HMCSs is due to chemical incorporation of arylsulfonic acid groups to HMCSs framework *via* diazonium coupling. Therefore, $ArSO_3H$-HMCSs work effectively as recyclable solid acid catalysts in the synthesis of ethyl levulinate from biomass-derived platform molecules.

4. Conclusions

Arylsulfonic acid functionalized hollow mesoporous carbon spheres, $ArSO_3H$-HMCSs, prepared by hard template approach combined with diazonium coupling, exhibit excellent heterogeneous acid catalytic activity and stability in the synthesis of ethyl levulinate from esterification of levulinic acid or ethanolysis of furfuryl alcohol. The inherent strong Brønsted acidity of $ArSO_3H$-HMCSs plays the paramount role to the catalytic activity; meanwhile, unique hollow spherical morphology with thin shell and excellent textural properties can shorten the diffusion distance and facilitate mass transport of the reactants and products. All of the above advantages can increase the accessibility of $ArSO_3H$ sites to the reactant molecules, leading to the increased acid catalytic activity to both target reactions compared with their ordered mesoporous analogs as well as sulphonated bulk carbon materials.

Acknowledgements

This work is supported by the Natural Science Fund of China (21173036; 51278092; 51308097; 51478095). Also, the work is supported by the Program for New Century Excellent Talents in University of Ministry of Education of China (NCET-13-0723).

Appendix A. Supplementary data

Supplementary data associated with this article can be found, in the online version, at http://dx.doi.org/10.1016/j.apcatb.2015.05.047

References

[1] Z.H. Zhang, K. Dong, Z.B. Zhao, ChemSusChem 4 (2011) 112–118.
[2] L. Hu, G. Zhao, W.W. Hao, RSC Adv. 2 (2012) 11184–11206.
[3] D.M. Alonso, J.Q. Bond, J.A. Dumesci, Green Chem. 12 (2010) 1493–1513.
[4] J.N. Chheda, G.W. Huber, J.A. Dumesic, Angew. Chem. Int. Ed. 46 (2007) 7164–7183.
[5] H. Joshi, B.R. Moser, J. Toler, W.F. Smith, T. Walker, Biomass Bioenergy 35 (2011) 3262–3266.
[6] H. Guo, Y. Lian, L. Yan, X. Qi, R.L. Smith, Green Chem. 15 (2013) 2167–2174.
[7] C.J. Barrett, J.N. Chheda, G.W. Huber, J.A. Dumesic, Appl. Catal. B: Environ. 66 (2006) 111–118.
[8] P. Gallezot, Chem. Soc. Rev. 41 (2012) 1538–1558.
[9] K. Jacobson, R. Gopinath, L.C. Meher, A.K. Dalai, Appl. Catal. B: Environ. 85 (2008) 86–91.
[10] L. Xu, W. Li, J. Hu, X. Yang, Y. Guo, Appl. Catal. B: Environ. 90 (2009) 587–594.
[11] E. Lam, J.H.T. Luong, ACS Catal. 4 (2014) 3393–3410.
[12] M. Hara, Energy Environ. Sci. 3 (2010) 601–607.
[13] K. Nakajima, M. Hara, ACS Catal. 2 (2012) 1296–1304.
[14] F. Su, Y.H. Guo, Green Chem. 16 (2014) 2934–2957.
[15] M. Toda, A. Takagaki, M. Okamura, J.N. Kondo, S. Hayashi, K.M. Domen, Hara, Nature 438 (2005) 178.
[16] M. Okamura, A. Takagaki, M. Toda, J.N. Kondo, T. Tatsumi, K. Domen, M. Hara, S. Hayashi, Chem. Mater. 18 (2006) 3039–3045.
[17] M. Hara, T. Yoshida, A. Takagaki, T. Takata, J.N. Kondo, K. Domen, S. Hayashi, Angew. Chem. Int. Ed. 43 (2004) 2955–2958.
[18] S. Suganuma, K. Nakajima, M. Kitano, D. Yamaguchi, H. Kato, S. Hayashi, M. Hara, J. Am. Chem. Soc. 130 (2008) 12787–12793.
[19] J. Dhainaut, J.P. Dacquin, A.F. Lee, K. Wilson, Green Chem. 12 (2010) 296–303.
[20] J. Du, X.Y. Lai, N.L. Yang, J. Zhai, D. Kisailus, F.B. Su, D. Wang, L. Jiang, ACS Nano 5 (2011) 590–596.
[21] C.C. Li, J. Dou, L.W. Chen, J.Y. Lin, H.C. Zeng, ChemCatChem 4 (2012) 1675–1682.
[22] L. Qin, X.X. Pan, L. Wang, X.P. Sun, G.L. Zhang, X.W. Guo, Appl. Catal. B: Environ. 150–151 (2014) 544–553.
[23] X. Zhang, H.X. Chen, Y.P. Xie, J.X. Guo, J. Mater. Chem. A 2 (2014) 3912–3918.
[24] F. Su, S. An, D. Song, X. Zhang, B. Lu, Y. Guo, J. Mater. Chem. A 2 (2014) 14127–14138.
[25] F. Su, L. Ma, D.Y. Song, X.H. Zhang, Y.H. Guo, Green Chem. 15 (2013) 885–890.
[26] L. Peng, L. Lin, J. Zhang, J. Shi, S. Liu, Appl. Catal. A: Gen. 397 (2011) 259–265.
[27] J.P. Lange, W.D. Graaf, R.J. Haan, ChemSusChem 2 (2009) 437–441.
[28] D.R. Fernandes, A.S. Rocha, E.F. Mai, C.J.A. Mota, V.T. Silva, Appl. Catal. A: Gen. 425–426 (2012) 199–204.
[29] P. Carà, R. Ciriminna, N.R. Shiju, G. Rothenberg, M. Pagliaro, ChemSusChem 7 (2014) 835–840.

[30] K.Y. Nandiwale, P.S. Niphadkar, S.S. Deshpande, V.V. Bokade, J. Chem. Technol. Biotechnol. 89 (2014) 1507–1515.
[31] P. Neves, M.M. Antunes, P.A. Russo, J.P. Abrantes, S. Lima, A. Fernandes, M. Pillinger, S.M. Rocha, M.F. Ribeiro, A.A. Valente, Green Chem. 15 (2013) 3367–3376.
[32] J.A. Melero, G. Morales, J. Iglesias, M. Paniagua, B. Hernández, S. Penedo, Appl. Catal. A: Gen. 466 (2013) 116–122.
[33] L.M. Guo, L.X. Zhang, J.L. Shi, Mater. Lett. 65 (2011) 1–3.
[34] B. Chang, J. Fu, Y. Tian, X. Dong, J. Phys. Chem. C 117 (2013) 6252–6258.
[35] J.A. Melero, G.D. Stucky, R. Griekena, G. Morales, J. Mater. Chem. 12 (2002) 1664–1670.
[36] N. Tsubouchi, C. Xu, Y. Ohtsuka, Energy Fuels 17 (2003) 1119–1125.
[37] B. Yi, R. Rajagopalan, H.C. Foley, U.J. Kim, X.M. Liu, P.C. Eklund, J. Am. Chem. Soc. 128 (2006) 11307–11313.
[38] Z.C. Yang, Y. Zhang, J.H. Kong, S.Y. Wong, X. Li, J. Wang, Chem. Mater. 25 (2013) 704–710.
[39] C.A. Dyke, J.M. Tour, J. Am. Chem. Soc. 125 (2003) 1156–1157.
[40] L.J. Konwar, P. Mäki-Arvela, E. Salminen, N. Kumar, A.J. Thakur, J. Mikkol, D. Deka, Appl. Catal. B: Environ. 176 (2015) 20–35.
[41] X.L. Wei, Macromolecules 32 (1999) 3114–3117.
[42] A.M. Puziya, O.I. Poddubnayaa, R.P. Sochab, J. Gurgulb, M. Wisniewskic, Carbon 46 (2008) 2113–2123.
[43] F. Liu, J. Sun, Q. Sun, L. Zhu, L. Wang, X. Meng, C. Qi, F.S. Xiao, Catal. Today 186 (2012) 115–120.
[44] Y.B. Huang, Y. Fu, Green Chem. 15 (2013) 1095–1111.
[45] D. Zuo, J. Lane, D. Culy, M. Schultz, A. Pullar, M. Waxman, Appl. Catal. B: Environ. 129 (2013) 342–350.
[46] J.A. Melero, J. Igesias, G. Morales, Green Chem. 11 (2009) 1285–1308.